

Persulfate Assisted Sonocatalytic Process for the Degradation of Reactive Yellow 145 Dye in Aqueous Solution

Özkan GÖRMEZ^{1*} 

¹Mersin University, Science Faculty, Chemistry Department, Mersin, Türkiye
 Özkan GÖRMEZ ORCID No: 0000-0002-1360-9275

*Corresponding author: ozkan.grmz@gmail.com

(Received: 17.11.2023, Accepted: 28.05.2024, Online Publication: 28.06.2024)

Keywords

Wastewater treatment, Sonocatalytic process, Box-Behnken Design, Azo dyes

Abstract: Pollutants resulting from industrial wastewater significantly threaten environmental health. Purification of wastewater, especially from the synthetic dye industry, is of great importance for the protection of aquatic systems. Advanced oxidation processes (AOPs), which are among the methods used in wastewater treatment in recent years, provide effective degradation of persistent organic pollutants with the help of radical species produced from oxidants used in the experimental environment.

In this study, the removal of synthetically prepared reactive yellow 145 (RY145) dye solution by the sonocatalytic method, one of the AOPs, in the presence of $(\text{Mn}_{0.37}\text{Fe}_{0.63})_2\text{O}_3$ catalyst and using persulfate as oxidant was examined. Characterization of the $(\text{Mn}_{0.37}\text{Fe}_{0.63})_2\text{O}_3$ catalyst synthesized by the sol-gel method was carried out by XRD, SEM and EDS techniques. While persulfate concentration (5-10 mM), time (2-5 h) and catalyst dosage ($0.25-0.75 \text{ g L}^{-1}$) were determined as experimental parameters for the oxidation of RY145 dye, Box-Behnken design was preferred for modeling the experimental study. In experimental studies, the maximum %TOC removal was calculated as 92.98% after 5 h at 10 mM PS and 0.75 g L^{-1} catalyst dosage.

69

Reaktif Sarı 145 Boyasının Sulu Çözeltisinin Persülfat Destekli Sonokatalitik Proses ile Degradasyonu

Anahtar Kelimeler

Atık su arıtımı, Sonokatalitik proses, Box-Behnken Tasarımı, Azo boyar maddeler

Öz: Endüstriyel atık sulardan kaynaklanan kirleticiler çevre sağlığını önemli ölçüde tehdit etmektedir. Özellikle boya endüstrisinden kaynaklanan atık suların arıtılması, sucul sistemlerin korunması açısından büyük önem taşımaktadır. Atıksu arıtımında son yıllarda kullanılan yöntemler arasında yer alan ileri oksidasyon prosesleri (AOP'ler), deney ortamında kullanılan oksidanlardan üretilen radikal türler yardımıyla kalıcı organik kirleticilerin etkin bir şekilde parçalanmasını sağlamaktadır.

Bu çalışmada, reaktif sarı 145 (RY145) boyası içeren sentetik olarak hazırlanmış atık suyun, $(\text{Mn}_{0.37}\text{Fe}_{0.63})_2\text{O}_3$ katalizörü varlığında ve oksidant olarak persülfat kullanılarak AOP tekniklerinden biri olan sonokatalitik yöntemle giderimi incelenmiştir. Sol-jel yöntemiyle sentezlenen $(\text{Mn}_{0.37}\text{Fe}_{0.63})_2\text{O}_3$ katalizörünün karakterizasyonu XRD, SEM ve EDS teknikleriyle gerçekleştirilmiştir. RY145 boyasının oksidasyonunda deneysel parametreler olarak persülfat konsantrasyonu (5-10 mM), süre (2-5 saat) ve katalizör dozajı ($0.25-0.75 \text{ g L}^{-1}$) belirlenirken, deneysel çalışmanın modellenmesinde Box-Behnken tasarımı tercih edilmiştir. Deneysel çalışmalarda 10 mM PS ve 0.75 g L^{-1} katalizör dozajında 5 saat sonra maksimum %TOC giderimi %92,98 olarak hesaplanmıştır.

1. INTRODUCTION

In parallel with the development of industry, it has become necessary to develop methods for the effective

treatment of toxic compounds that cause environmental pollution without being released into natural water cycles [1]. Various synthetic dyes used in textile factories may cause changes in the oxygen content and temperature of

the water as a result of mixing with water, as well as causing a significant environmental hazard due to toxic species released as a result of hydrolysis, oxidation and/or other bio-chemical reactions of these dyes [2-4]. Therefore, effective methods must be applied to remove dyes from the aquatic environment. The processes applied to remove azo dyes from aqueous solutions are divided into three parts. These are respectively (i) physical; (ii) biological and (iii) chemical methods. Physical methods are generally based on the mass transfer mechanism or simple separation of dyes from aqueous solutions. Biological techniques require the use of microorganisms in the degradation process of azo dyes. In chemical methods, azo dyes are converted into degradation products by using various chemicals and theories. Physical methods are mainly classified as adsorption, filtration, ion exchange, coagulation, sedimentation and membrane separation. Chemical methods are generally grouped under Advanced oxidation techniques. Advanced oxidation techniques include many techniques such as Fenton and Fenton-based methods, Electro-oxidation, Ozonation, sonolysis, photolysis, and photocatalysis [5].

Reactive dyes included in synthetic textile dyes can be covalently bonded to the fiber structure thanks to the sulfonic group in their molecules and are highly water-soluble structures [3,6]. Another classification for synthetic dyes is azo dyes. Azo dyes have azo groups (-N=N-) in a complex aromatic structure. The deep color of these dyes is due to the azo group, and the color may disappear with the degradation of this group [7-9]. Reactive yellow 145 (RY145) dye, which contains azo group and monochlorotriazine, is generally used in cotton dyeing [6,10] and various physical and chemical techniques have been used to remove this dye from wastewater. To adsorption-based removal of RY145, various adsorbents such as watermelon seeds [6], KOH-activated biochar [11], eggshell waste [12], soybean hull [13], $\text{MnO}_x\text{-CeO}_2$ [6], zero-valent iron/(Fe-Mn) binary oxide/bentonite nanocomposite [14] have been used previous studies. Although the adsorption method is low-cost and simple operation, it cannot completely eliminate the pollutant. Recently, advanced oxidation methods based on reactive oxygen species (ROS) formation, especially hydroxyl radical ($\cdot\text{OH}$), have been used in the oxidation of refractory organic pollutants that cannot be completely removed in biological treatment, such as textile dyestuffs [15]. In previous studies, $\text{Ni}_3\text{O}_4\text{-Co}_3\text{O}_4/\text{Al}_2\text{O}_3$ [8], Co-Fe BTC/graphitic carbon nitride [16], nano CuO [17], nano- TiO_2 [18], $\text{Al}_2\text{O}_3/\text{ZrO}_2$ [19], $\text{Co}_{1-x}\text{Zn}_x\text{Fe}_2\text{O}_4$ nanodot coated with polyaniline [20], $\alpha\text{-Fe}_2\text{O}_3@\text{C}@\text{SiO}_2/\text{TiO}_2$ [21] nanocomposite etc. photocatalysts were developed for the oxidation of the synthetic aqueous solution of RY145 dye and their effectiveness in photocatalytic oxidation was examined. In recent years, applications of sulfate radical-based processes have attracted attention. Sulfate radical ($\text{SO}_4^{\cdot-}$) formation is produced as a result of thermal, UV and metal ions (metal oxides) supported activations for the homolytic breaking of the peroxide (O-O) bond of persulfate (PS) and peroxymonosulfate (PMS) structures. Since hydroxyl ($\cdot\text{OH}$, $E^\circ=2.80$ V vs SCE), and sulfate radicals ($\text{SO}_4^{\cdot-}$, $E^\circ=2.5\text{-}3.1$ V vs SCE) have very high

oxidation potential, they react with organic pollutants non-selectively and at very high rates [22].

Sonochemical degradation (sonolysis) is used in support of other AOPs as well as being used alone. Applications based on sonolysis include sonocatalysis [23], sono/Fenton [24], sonication-ozonation [25], sonophotocatalysis [26], sonoelectrochemical oxidation [27] processes. Acoustic cavitation occurs due to compression and rarefaction cycles caused by ultrasonic emissions during sonolysis. The positive pressure caused by a large number of cavitation bubbles causes local high temperatures (5000 K) and high pressures (500 atm) in the solution, like a microreactor. Among the ROS formed in these local regions, there are also significant amounts of hydroxyl radicals [28-30]. Although, the most important disadvantages of the sonolysis process seem to be relatively long process time and energy consumption, the use of different catalysts and oxidants that have emerged recently are effective in solving these problems [31].

Bixbyite ($\text{Fe,Mn})_2\text{O}_3$ and hematite ($\text{Fe}_{2-x}\text{Mn}_x\text{O}_3$), which are manganese iron oxide structures, are stable phases at low temperatures, whereas the spinel phase ($\text{Fe,Mn})_3\text{O}_4$ shows stability at higher temperatures [32]. It is also possible to obtain mixtures of these phase types at intermediate temperatures [33,34]. There may be different Mn/Fe molar ratios in the bixbyite structure depending on the synthesis conditions. The bixbyite-manganese iron oxide structure has been mostly studied as an oxygen storage material. Manganese iron oxide structures in bixbyite phase are mechanically durable and inexpensive oxygen-carrier materials that are suitable for chemical looping with oxygen uncoupling (CLOU) in the air reactor [33]. These types of storage materials undergo a reversible redox reaction with oxygen.

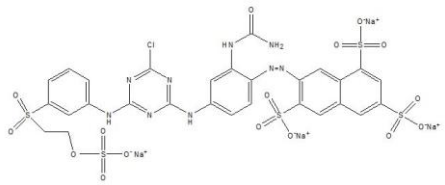
In this study, persulfate-assisted sonocatalytic oxidation of RY145 dye using manganese iron oxide ($\text{Mn}_{0.37}\text{Fe}_{0.63})_2\text{O}_3$ catalyst was examined. The effects of persulfate concentration, time and catalyst dosage on the oxidation of RY145 dye were examined using the response surface method and Box-Behnken design (BBD), and the optimum conditions were determined.

2. MATERIAL AND METHOD

2.1. Materials

Reactive yellow 145 (RY145) was supplied from EKSOY Company (Adana, Türkiye) (Table 1). Potassium persulfate ($\text{K}_2\text{S}_2\text{O}_8$), citric acid ($\text{C}_6\text{H}_8\text{O}_7$), $\text{Mn}(\text{NO}_3)_2\cdot 4\text{H}_2\text{O}$, and $\text{Fe}(\text{NO}_3)_3\cdot 9\text{H}_2\text{O}$ were purchased from Merck.

Table 1. Structure and properties of RY145 dye [35].

Properties of RY145	
Structure	
Molecular Formula	C ₂₈ H ₂₀ ClN ₉ Na ₄ O ₁₆ S ₅
Molecular Weight	1026.25 g mol ⁻¹
CAS Registry Number	93050-80-7
Water solubility	80 g L ⁻¹

2.2. Method

2.2.1. Synthesis of catalyst

In the synthesis of manganese^{III}-iron^{III} oxide ((Mn_{0.37}Fe_{0.63})₂O₃) structures, the sol-gel method was used to prepare Fe:Mn molar ratios of 1.7:1. Briefly, metal salts containing 0.17 mol Fe³⁺ and 0.1 mol Mn²⁺ were mixed in deionized pure water until completely dissolved. To this homogeneous mixture, 0.27 mol citric acid solution was added dropwise so that the metal ions: citric acid molar ratio was 1:1. It was waited in the magnetic stirrer at 70 °C until the gel formed, and then it was placed in a porcelain crucible and calcined at 700 °C for 5 h.

2.2.2. Sonocatalytic oxidation

The sonocatalytic experiments were carried out in capped pyrex glass bottles with a capacity of 150 mL. Catalyst and persulfate were added to 100 mL of 50 mg L⁻¹ RY145 solution and placed in an ultrasonic bath (Bandelin Sonorex, 84 W, 40 kHz). The temperature was kept constant at 30 °C by water circulation.

2.2.3. Experimental design

Box-Behnken design was used for the optimization study in the sonocatalytic oxidation of RY145 dyestuff. The most commonly used BBD for second order models in the surface method is a 3-level (-1, 0, +1) design. While persulfate (PS) concentration (X_1), time (X_2), and catalyst dosage (X_3) were selected as independent variables, TOC removal was followed as the dependent variable, that is the response (Y). The lowest (-1) and highest level (+1) ranges for the three independent variables were selected as 5-10 mM PS, 2-5 h, and 0.25-0.75 g L⁻¹ (Mn_{0.37}Fe_{0.63})₂O₃ catalyst (Table 2). The BBD with 3 independent variables (k) was created as a matrix of 17 runs (N) based on the $N=2k \times (k-1) + C_0$ formula (where C_0 is the number of central points) by the Design-Expert

11 program. The equation of quadratic equation showing the correlation between the independent variables and the response is as follows (Equation (1)).

$$Y = \beta_0 + \sum_{i=1}^k \beta_i X_i + \sum_{i=1}^k \beta_{ii} X_i^2 + \sum_i \sum_j \beta_{ij} X_i X_j + \varepsilon \quad (1)$$

where, X_i and X_j point out the independent variables, ε represents the random error, β_0 , β_i , β_{ii} and β_{ij} are the constant coefficient, the linear coefficient, the quadratic coefficient and the interaction coefficient, respectively.

2.2.4. Determination of total organic carbon content

Total organic carbon (TOC) contents of the samples taken were determined using the Merck TOC cell test. After the samples were heated at 120 °C for 2 h and were left for 1 h to cool. Afterwards, TOC content was measured with a Spectroquant NOVA 30 model photometer (Merck).

2.2.5. Characterization of catalyst

Crystal structure analysis of manganese iron oxide was performed by X-Ray powder Diffractometry (XRD, Rigaku SmartLab model) using Cu-K $\alpha_{1,2}$ radiation at 40 kV from 20° to 70° at the scan rate of 2°/min. Field Emission Scanning Electron Microscopy (Fe-SEM, Zeiss Supra 55) was used to determine the morphology of the catalyst using Pt coating. Also, surface element distribution was examined with the Energy Dispersive Spectrometry (SEM-EDS) system.

3. RESULTS AND DISCUSSION

3.1. Characterization of Manganese Iron Oxide

The SEM images of the (Mn_{0.37}Fe_{0.63})₂O₃ catalyst is given in Figure 1a, b. It is similar to the literature in terms of morphological structure [34]. Moreover, the elemental composition and atomic distribution of the manganese iron oxide catalyst are depicted in the EDS spectrum in Figure 1c.

According to the XRD pattern given in Figure 1d, the presence of specific diffraction peaks (ICDD PDF-2, 01-071-0637) belonging to the cubic bixbyite ((Mn,Fe)₂O₃) manganese iron oxide structure is seen due to, as well as the diffraction peaks of the hematite phase as an impurity [33]. Herein, XRD pattern supports bixbyite ((Mn_{0.37}Fe_{0.63})₂O₃) structure with 37% Mn and 63% Fe molar fraction. The lattice parameter of the synthesized magnesium iron oxide structure corresponds to $a = b = c = 9.41 \text{ \AA}$ and $\alpha = \beta = \gamma = 90^\circ$, and the formation of a strong cubic lattice structure is observed.

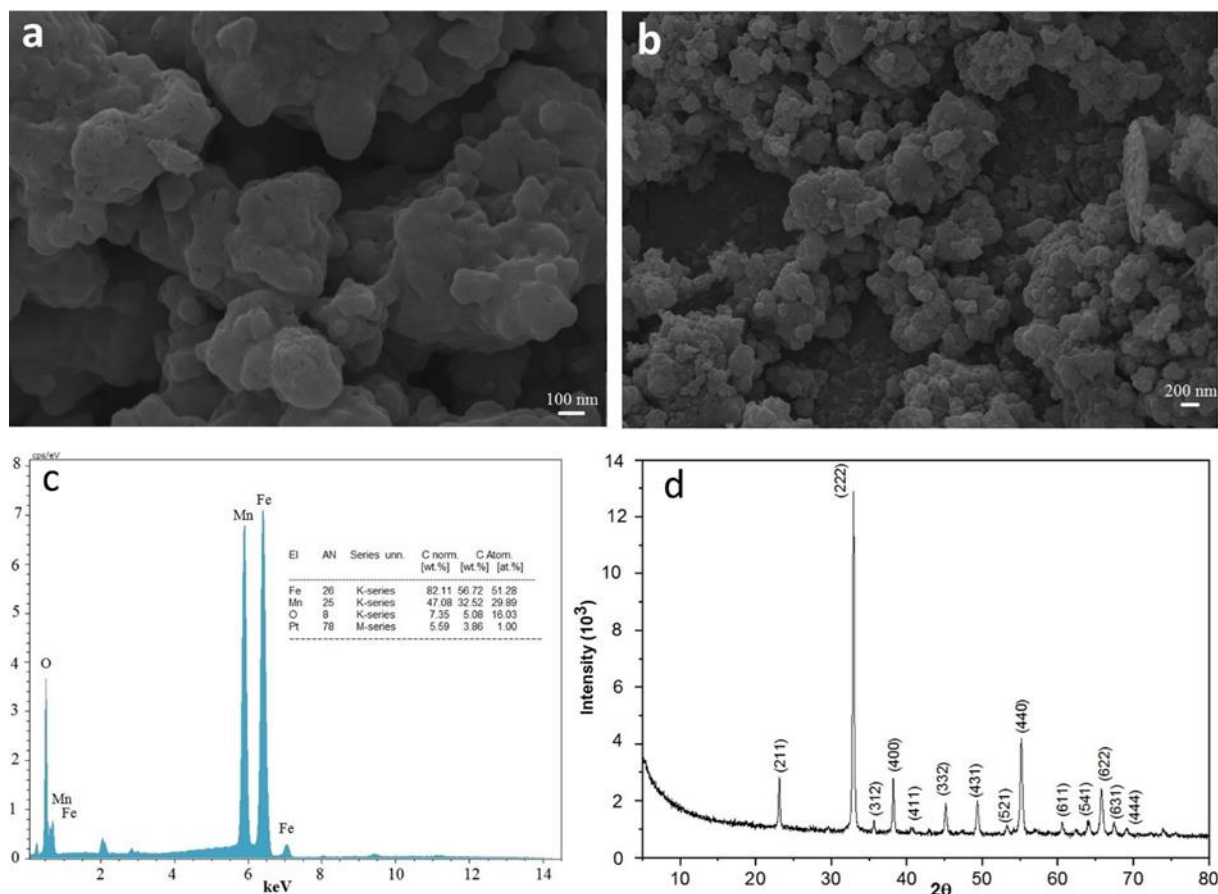


Figure 1. SEM images (a, b), EDS spectrum (c), and XRD pattern of catalyst (d).

3.2. Persulfate Assisted Sonocatalytic Oxidation of RY145

The effects of sonolysis (US), persulfate-assisted sonolysis (US/PS), sonocatalysis (US/Catalyst), and persulfate-assisted sonocatalysis (US/PS/Catalyst) processes on the oxidation of RY145 dye solution were monitored by the decrease in TOC content. While it was observed that sonolysis alone and PS-assisted sonolysis methods were not effective on TOC removal, 18% and 58% TOC removal was achieved with sonocatalytic and PS-assisted sonocatalytic methods, respectively. The combination of sonolysis with other systems creates a synergistic effect for radical formation and oxidation of organic pollutants. In sonolysis applications, especially magnetic catalysts can be distributed more homogeneously in the solution, thus increasing the effective surface area.

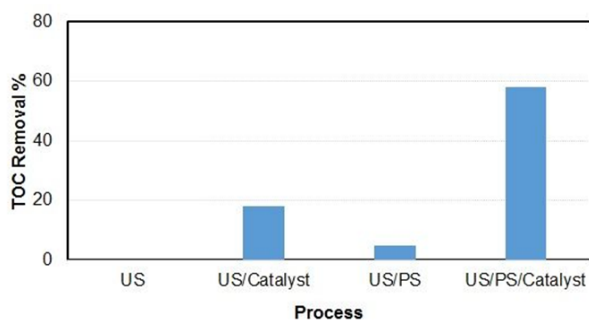
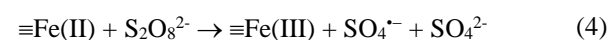
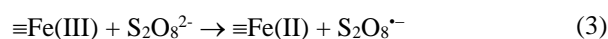
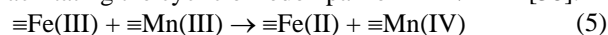


Figure 2. TOC removal of RY145 solution at different processes (Catalyst: 0.25 g L⁻¹, PS: 5 mM, t= 3.5 h).

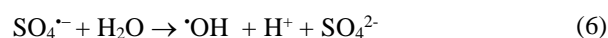
In order for the sulfate radical to form through heat activation, the temperature must be between 40-120 °C, because to break of peroxide (O-O) bond requires 140 - 213.3 kJ mol⁻¹ a thermal activation energy [36]. Whereas, persulfate activation is carried out with transition metal ions and the formation of sulfate radical is achieved by Equations (2-4) at moderate temperatures [37].



Herein, the higher standard redox potential of Fe³⁺/Fe²⁺ ($E^\circ = 0.77$ V vs SHE) allows for the oxidation of Mn³⁺ to Mn⁴⁺ ($E^\circ = 0.15$ V) as giving Equation (5) and results in facilitating the cyclic of redox pair of Mn⁴⁺/Mn³⁺ [38].



At all pH values, the formation of hydroxyl radicals may occur as a result of the reaction of the sulfate radical with water due to Equation (6) [39]. For this reason, it would be more accurate to accept the presence of both hydroxyl and sulfate radicals in the bulk solution.



The effects of persulfate, catalyst concentration and time on the sonocatalytic oxidation of RY145 solution at close to room temperature were examined using the Box-Behnken design, the experimental matrix and results are given in Table 2.

Table 2. BBD matrix for RY145 oxidation.

Run no	X_1 PS (mM)	X_2 Time (h)	X_3 Catalyst (g L ⁻¹)	TOC Removal (%)
1	5 (-1)	5 (+1)	0.50 (0)	76.82
2	15 (+1)	3.5 (0)	0.25 (-1)	66.23
3	5 (-1)	3.5 (0)	0.75 (+1)	73.72
4	15 (+1)	3.5 (0)	0.75 (+1)	81.25
5	10 (0)	2 (-1)	0.25 (-1)	59.33
6	10 (0)	3.5 (0)	0.50 (0)	82.12
7	5 (-1)	2 (-1)	0.50 (0)	51.82
8	10 (0)	3.5 (0)	0.50 (0)	84.28
9	10 (0)	5 (+1)	0.75 (+1)	92.98
10	10 (0)	3.5 (0)	0.50 (0)	79.02
11	10 (0)	2 (-1)	0.75 (+1)	70.33
12	10 (0)	3.5 (0)	0.50 (0)	85.36
13	5 (-1)	3.5 (0)	0.25 (-1)	58.54
14	10 (0)	5 (+1)	0.25 (-1)	81.62
15	15 (+1)	2 (-1)	0.50 (0)	62.61
16	10 (0)	3.5 (0)	0.50 (0)	82.26
17	15 (+1)	5 (+1)	0.50 (0)	88.21

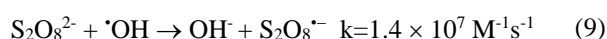
In ANOVA, the F -value (40.69) and p -value (<0.0001) of the proposed quadratic model (Table 3) for the sonocatalytic oxidation of RY145 dye solution shows an excellent fit to the experimental results. The compatibility of the model with the experimental results was also supported by the correlation coefficient values, R^2 and adjusted R^2 , these values are 0.9812 and 0.9571, respectively. In the proposed quadratic model, the most effective terms according to their p -values (<0.05) are the linear (X_1 , X_2 , X_3) and quadratic (X_1^2 , X_2^2 , X_3^2) terms of the three independent variables. In contrast, the interactive effects of the independent variables do not have a significant effect on the TOC removal efficiency. When the polyfunctional Equation (7) of the quadratic model is examined, when linear terms have a positive effect, quadratic terms have a negative effect on the response. In other words, as all three independent variables increase up to a certain level, they have a positive effect on the response, but after the optimum point, their effect decreases or becomes constant (Figure 3).

Table 3. ANOVA results of BBD for sonocatalytic oxidation of RY145

Source	Sum of Squares	df	Mean Square	F value	P value	
Model	2163.18	9	240.35	40.69	< 0.0001	significant
X_1 -PS (mM)	174.85	1	174.85	29.60	0.0010	
X_2 -time (h)	1140.99	1	1140.99	193.18	< 0.0001	
X_3 -Catalyst (g L ⁻¹)	345.32	1	345.32	58.47	0.0001	
X_1X_2	0.0900	1	0.0900	0.0152	0.9052	
X_1X_3	0.0064	1	0.0064	0.0011	0.9747	
X_2X_3	0.0324	1	0.0324	0.0055	0.9430	
X_1^2	374.94	1	374.94	63.48	< 0.0001	
X_2^2	46.03	1	46.03	7.79	0.0268	
X_3^2	44.10	1	44.10	7.47	0.0292	
Residual	41.34	7	5.91			
Lack of Fit	17.74	3	5.91	1.00	0.4781	not significant
Pure Error	23.60	4	5.90			
Cor Total	2204.53	16				

$$\begin{aligned} \text{TOC Removal (\%)} = & 82.61 + 4.67X_1 + \\ & 11.94X_2 + 6.57X_3 + 0.15X_1X_2 - 0.04X_1X_3 \\ & + 0.09X_2X_3 - 9.44X_1^2 - 3.31X_2^2 - 3.24X_3^2 \end{aligned} \quad (7)$$

Figure 3 shows the interactive effects of PS concentration, catalyst dosage, and process time, which are effective in the PS-assisted sonocatalytic oxidation of RY145 dye, when a variable is kept constant. When Figure 3a is examined, it is seen that the processing time is an important parameter, and an effective TOC removal efficiency can be achieved especially after 4 h. A significant increase in TOC removal was observed when the PS oxidant concentration was increased up to 11 mM, but the efficiency started to decrease as it increased above 11 mM. When the PS concentration was 5 mM, TOC removal enhanced to 79%, whereas the PS concentration was increased to 11 and 15 mM the efficiency was observed as 94% and 89%, respectively. The reason for this result is that excess PS in the medium acts as a radical scavenger and consumes the radicals created during the process via Equations (8) and (9) [40].



In case the effect of catalyst dosage on TOC removal was examined in Figures 3b and 3c, 82% TOC removal was achieved with 0.25 g L⁻¹ catalyst at 5 h and 11 mM PS. Increasing the catalyst dosage to 0.6 g L⁻¹ increased TOC removal to 94% as it provided more active surfaces involved in radical formation. Keeping the catalyst dosage at 0.75 g L⁻¹ and determining TOC removal as 95% under the same conditions showed that there was no need to increase the catalyst dosage further.

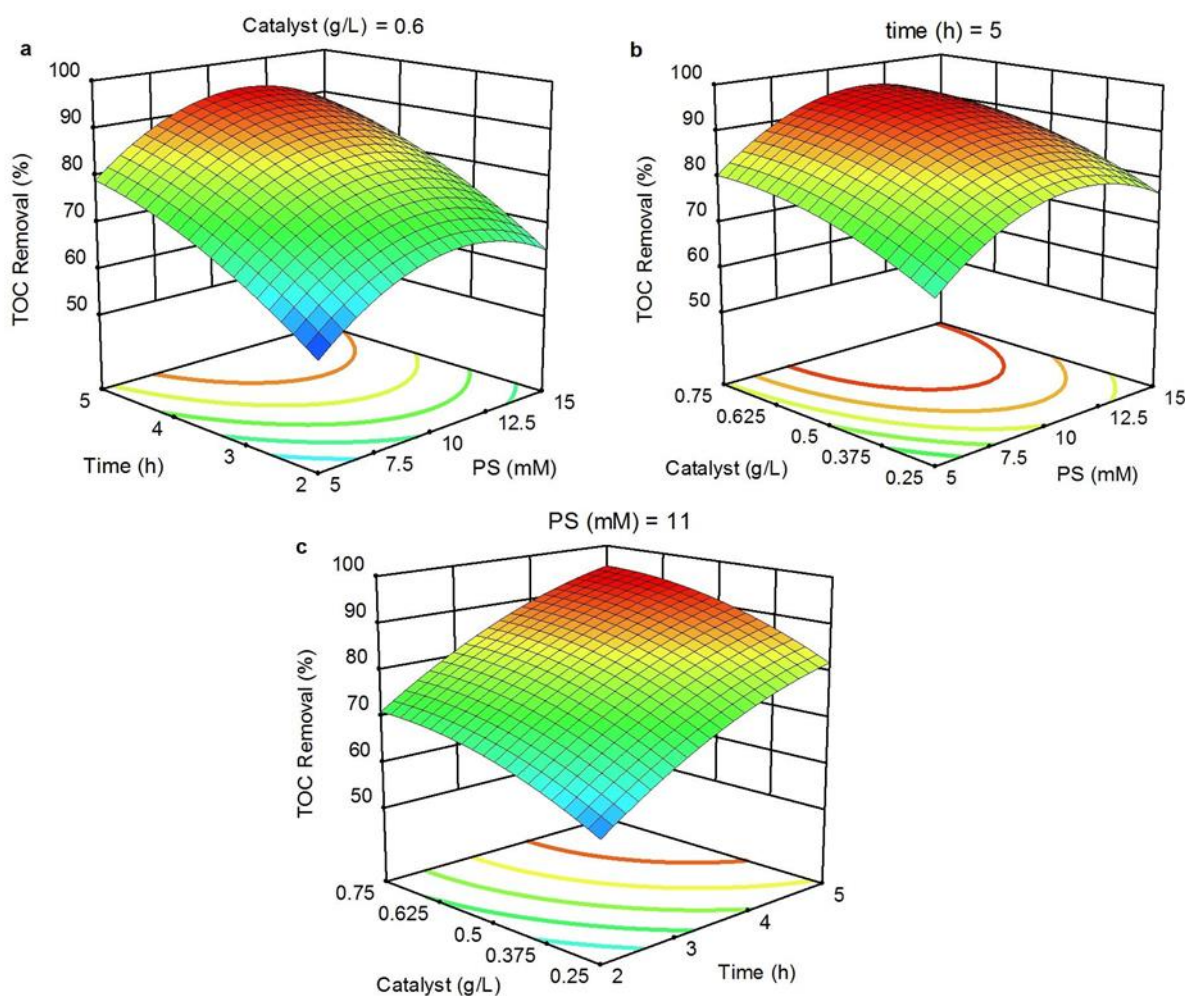


Figure 3. The effect of time and PS concentration (a), catalyst dosage and PS concentration (b), and catalyst dosage and time on TOC removal efficiency (pH 5.5).

According to the response surface method, the optimum conditions to achieve 95% TOC removal were determined as follows: 11 mM PS, 5 h process time, and 0.7 g L^{-1} catalyst dosage. After the magnetic catalyst was collected with an external magnet and washed with ethanol and water, its reuse was tested for five runs, and 95% TOC removal was achieved in each cycle.

Mohammad et al. [8], reported that the color removal of 50 mg L^{-1} RY145 aqueous solution was completed in 60 min at pH 3 with a catalyst dosage of 0.1 g L^{-1} with the $\text{Ni}_3\text{O}_4\text{-Co}_3\text{O}_4/\text{Al}_2\text{O}_3$ photocatalyst. Nguyen et al. [17], achieved 99% color removal and 46% TOC removal for 50 mg/L of RY145 in 45 min by using bimetallic Co-Fe BTC/graphitic carbon nitride nanocomposite photocatalyst. Vu et al. [41], achieved 98% color removal of RY145 (100 mg L^{-1}) as a result of 60-min photocatalysis using the e-BTC/Graphene oxide (GO)-30 composite synthesized by microwave-assisted hydrothermal method. In the another study where Ag-Zn-BTC/GO composite was used as the photocatalyst, COD, BOD and TOC removals were reported as 80.06%, 81.66% and 56.13%, respectively, as a result of photocatalytic oxidation of 65 mg L^{-1} RY145 aqueous solution for 35 min [42]. When the previous studies are examined, it can be seen that more emphasis is placed on color removal. In this study, 100%

color removal as well as 95% TOC removal for RY145 dye was achieved using the PS-assisted sonocatalytic method at 5 h.

4. CONCLUSION

In the study, experimental modeling was made with the Box-Behnken design, persulfate was used as the oxidant and $(\text{Mn}_{0.37}\text{Fe}_{0.63})_2\text{O}_3$ was used as the catalyst in the sonocatalytic degradation process of RY145 dye. The maximum TOC removal value during experimental studies was 92.98%. However, according to the second-order model obtained with the Box-Behnken design, the optimum conditions were determined as 11 mM PS, 5 h of processing time and 0.7 g L^{-1} catalyst dosage, and the TOC removal value to be obtained under these conditions was calculated as 95%. It has been determined that $(\text{Mn}_{0.37}\text{Fe}_{0.63})_2\text{O}_3$ used as a catalyst can be easily separated from the experimental environment due to its magnetic properties and maintains its catalytic activity even when reused 5 times. The obtained ANOVA datas such as F-value, R^2 and $\text{Adj-}R^2$ of the applied quadratic model prove the high compatibility of the obtained results with each other. The quadratic equation obtained for the removal of RY145 dye in the study can be used as preliminary data in determining experimental conditions for similar studies

to be carried out in this field. Considering the whole study, it has been shown that AOPs techniques, whose effectiveness has been demonstrated in many studies, can be applied in perfect harmony with experimental modeling methods.

REFERENCES

- [1] Arefi-Oskoui S, Khataee A, Behrouz SJ, Vatanpour V, Gharamaleki SH, Orooji Y, et al. Development of MoS₂/O-MWCNTs/PES blended membrane for efficient removal of dyes, antibiotic, and protein. *Sep. Purif. Technol.* 2022;280:119822.
- [2] Deveci İ, Mercimek B. Performance of SiO₂/Ag Core/Shell particles in sonocatalytic degradation of Rhodamine B. *Ultrason. Sonochem.* 2019;51:197-205.
- [3] Miladinova PM, Lukanova VR. Investigations on the dyeing ability of some reactive triazine azo dyes containing tetramethylpiperidine fragment. *J. Chem. Technol. Metall.* 2017;52(1):3-12.
- [4] Karaman C, Karaman O, Show PL, Orooji Y, Karimi-Maleh H, Utilization of a double-cross-linked amino-functionalized three-dimensional graphene networks as a monolithic adsorbent for methyl orange removal: equilibrium, kinetics, thermodynamics and artificial neural network modeling. *Environ. Res.* 2021;207:112156.
- [5] Kamenicka B. Chemical degradation of azo dyes using different reducing agents: A review. *J. Water Process Engin.* 2024;61:105350.
- [6] Gharbani P. Modeling and optimization of Reactive Yellow 145 dye removal process onto synthesized MnOX-CeO₂ using response surface methodology. *Colloids and Surfaces A* 2018;548:191-7.
- [7] Benkaddour S., Slimani R, Hiyane H, El Ouahabi I, Hachoumi I, El Antri S, et al. Removal of reactive yellow 145 by adsorption onto treated watermelon seeds: Kinetic and isotherm studies. *Sustain. Chem. Pharm.* 2018;10:16–21.
- [8] Mohammad EJ, Lafta AJ, Kahdim SH. Photocatalytic removal of reactive yellow 145 dye from simulated textile wastewaters over supported (Co, Ni)₃O₄/Al₂O₃ co-catalyst. *Pol. J. Chem. Technol.* 2016;18(3):1-9.
- [9] Raval NP, Shah PU, Shah NK. Malachite green “a cationic dye” and its removal from aqueous solution by adsorption. *Appl. Water Sci.* 2017;7:3407-3445.
- [10] Khurana I, Saxena A, Bharti, Khurana, JM, Rai PK. Removal of dyes using graphene-based composites: a review. *Water Air Soil Poll.* 2017;228:180-197.
- [11] Ullah F, Ji G, Irfan M, Gao Y, Shafiq F, Sun Y. Adsorption performance and mechanism of cationic and anionic dyes by KOH activated biochar derived from medical waste pyrolysis. *Environ. Pollut.* 2022;314:120271.
- [12] Ofudje EA, Sodiya EF, Ibadin FH, Ogundiran AA, Alayande SO, Osideko OA. Mechanism of Cu²⁺ and reactive yellow 145 dye adsorption onto eggshell waste as low-cost adsorbent. *Chem. Ecol.* 2021;37(3), 268-289.
- [13] Giordano EDV, Brassesco ME, Camiscia P, Picó GA, Valetti NW. A new alternative and efficient low-cost process for the removal of reactive dyes in textile wastewater by using soybean hull as adsorbent. *Water Air Soil Poll.* 2021;232:165.
- [14] Lam PV, Duong NB, Bich PTN, Trang, QTT. Adsorption removal of Reactive Yellow 145 dye from aqueous solution using novel nZVI/(Fe–Mn) binary oxide/bentonite nanocomposite. *Desalin. Water Treat.* 2022;280:168-176.
- [15] Khataee A, Gholami P, Vahid B, Joo SW. Heterogeneous sono-Fenton process using pyrite nanorods prepared by non-thermal plasma for degradation of an anthraquinone dye. *Ultrason. Sonochem.* 2016;32:357-370.
- [16] Nguyen MB, Sy DT, Thoa VTK, Hong NT, Doan HV. Bimetallic Co-Fe-BTC/CN nanocomposite synthesised via a microwave-assisted hydrothermal method for highly efficient Reactive Yellow 145 dye photodegradation. *J. Taiwan Inst. Chem. Eng.* 2022;140:104543.
- [17] Ebrahimzadeh-Rajaei G. Removal of reactive yellow 145 dye from aqueous solution by photocatalytic and sonocatalytic degradation in the presence of CuO nanocatalyst. *Theor. Found. Chem. Eng.* 2022;56:1088–1099.
- [18] Aksu M, Hasa M, Tanattı NP, Erden B, Katircioğlu Sınmaz G, Boysan F, et al. Assessment of photocatalytic n-TiO₂/UV and n-TiO₂/H₂O₂/UV methods to treat DB 86, RY 145 and AV 90 dye mix containing wastewater. *Desalin. Water Treat.* 2022;266:226-235.
- [19] Yaghoubi A, Ramazani A, Fardood ST. Synthesis of Al₂O₃/ZrO₂ nanocomposite and the study of its effects on photocatalytic degradation of Reactive Blue 222 and Reactive Yellow 145 dyes. *Chemistry Select* 2020;5:9966-9973.
- [20] Bashar MA, Molla MTH, Chandra D, Malitha MD, Islam MS, Rahman MS, et al. Hydrothermal synthesis of cobalt substitute zinc-ferrite (Co_{1-x}Zn_xFe₂O₄) nanodot, functionalised by polyaniline with enhanced photocatalytic activity under visible light irradiation. *Heliyon* 2023;9(4): e15381.
- [21] Mousavi SE, Younesi H, Bahramifar N, Tamunaidu P, Karimi-Maleh H. A novel route to the synthesis of α-Fe₂O₃@C@SiO₂/TiO₂ nanocomposite from the metal-organic framework as a photocatalyst for water treatment. *Chemosphere* 2022;297:133992.
- [22] Brillas E. Removal of insecticides from waters and soils by sulfate radical-based advanced oxidation processes. *Appl. Res.* 2023; e202300055.
- [23] Karaca S, Çakmak Önal E, Açıslı Ö, Khataee A. A literature review of ultrasound technology and its application in wastewater disinfection. *Mater. Chem. Phys.* 2021;260:124125.
- [24] Dindarsafa M, Khataee A, Kaymak B, Vahid B, Karimi A, Rahmani, A. Heterogeneous sono-Fenton-like process using martite nanocatalyst prepared by high energy planetary ball milling for treatment of a textile dye. *Ultrason. Sonochem.* 2017;34:389-399.
- [25] Wang B, Shi W, Zhang H, Ren HY, Xiong MY. Promoting the ozone-liquid mass transfer through external physical fields and their applications in

- wastewater treatment: A review. *J. Environ. Chem. Eng.* 2021;9(5):106115.
- [26] Joseph CG, Puma GL, Bono A, Krishnaiah D. Sonophotocatalysis in advanced oxidation process: A short review. *Ultrason. Sonochem.* 2009;16(5):583–589.
- [27] Ojo BO, Arotiba OA, Mabuba N. Sonoelectrochemical oxidation of sulfamethoxazole in simulated and actual wastewater on a piezopolarizable FTO/BaZr_xTi_(1-x)O₃ electrode: reaction kinetics, mechanism and reaction pathway studies. *RSC Adv.* 2022;12:30892-30905.
- [28] Liu P, Wu Z, Abramova AV, Cravotto G. Sonochemical processes for the degradation of antibiotics in aqueous solutions: A review. *Ultrason. Sonochem.* 2021;74:105566.
- [29] Yap HC, Pang YL, Lim S, Abdullah AZ, Ong HC, Wu CH. A comprehensive review on state-of-the-art photo-, sono-, and sonophotocatalytic treatments to degrade emerging contaminants. *Int. J. Environ. Sci. Technol.* 2019;16:601-628.
- [30] Sathishkumar P, Mangalaraja RV, Anandan S. Review on the recent improvements in sonochemical and combined sonochemical oxidation processes—A powerful tool for destruction of environmental contaminants. *Renew. Sust. Energ. Rev.* 2016;55:426–454.
- [31] Akdağ S, Rad TZ, Keyikoğlu R, Orooji Y, Yoon Y, Khataee A. Peroxydisulfate-assisted sonocatalytic degradation of metribuzin by La-doped ZnFe layered double hydroxide. *Ultrason. Sonochem.* 2022;91:106236.
- [32] Kjellqvist L, Selleby M. Thermodynamic assessment of the Fe-Mn-O system. *J. Phase Equilib. Diffus.* 2010;31:113-134.
- [33] Azimi G, Leion H, Rydén M, Mattisson T, Lyngfelt A. Investigation of different Mn–Fe oxides as oxygen carrier for Chemical-Looping with Oxygen Uncoupling (CLOU). *Energy and Fuels* 2013;27(1):367-377.
- [34] Wokon M, Kohzer A, Linder M. Investigations on thermochemical energy storage based on technical grade manganese-iron oxide in a lab-scale packed bed reactor. *Sol. Energy* 2017;153:200-214.
- [35] World dye variety [Cited 2023 Nov 15] Available from: (<https://www.worlddyevariety.com/reactive-dyes/reactive-yellow-145.html>).
- [36] Wang J, Wang S. Activation of persulfate (PS) and peroxymonosulfate (PMS) and application for the degradation of emerging contaminants. *Chem. Eng. J.* 2018;334:1502-1517.
- [37] Liu H, Bruton TA, Li W, Buren JV, Prasse C, Doyle FM, et al. Oxidation of benzene by persulfate in the presence of Fe(III)- and Mn(IV)-containing oxides: Stoichiometric efficiency and transformation products. *Environ. Sci. Technol.* 2016;50:890–898.
- [38] Deng Q, Zhang X, Chang L, Chai H, Huang Y. The MOF/LDH derived heterostructures Co₃O₄/MnCo₂O₄ composite for enhanced degradation of levofloxacin by peroxymonosulfate activation. *Sep. Purif. Technol.* 2022;294:121182.
- [39] Liang C, Wang ZS, Bruell CJ. Influence of pH in persulfate oxidation of TCE at ambient temperatures. *Chemosphere.* 2007;66(1):106-113.
- [40] Ren W, Huang X, Wang L, Liu X, Zhou Z, Wang Y., et al. Degradation of simazine by heat-activated peroxydisulfate process: A coherent study on kinetics, radicals and models. *Chem. Eng. J.* 2021;426:131876.
- [41] Vu HT, Nguyen MB, Vu TM, Le GH, Pham TTT, Nguyen TD, et al. Synthesis and application of novel nano Fe-BTC/GO composites as highly efficient photocatalysts in the dye degradation. *Topics in Catalysis* 2020;63:1046–1055.
- [42] Nguyen MB, Le GH, Nguyen TD, Nguyen QK, Pham TTT, Lee T, et al. Bimetallic Ag-Zn-BTC/GO composite as highly efficient photocatalyst in the photocatalytic degradation of reactive yellow 145 dye in water. *J. Hazard. Mater.* 2021;420:126560.